

# Phase-sensitive X-ray Diffraction Imaging of Defects in Biological Macromolecular Crystals

Z. W. Hu,<sup>1</sup> B. Lai,<sup>2</sup> Y. S. Chu,<sup>2</sup> Z. Cai,<sup>2</sup> D. C. Mancini,<sup>2</sup> B. R. Thomas,<sup>1</sup> A. A. Chernov<sup>1</sup>

<sup>1</sup>Universities Space Research Association, National Aeronautics and Space Administration (NASA)/  
Marshall Space Flight Center, Huntsville, AL, U.S.A.

<sup>2</sup>Advanced Photon Source, Argonne National Laboratory, Argonne, IL, U.S.A.

## Introduction

The characterization of defects and/or disorder presents much greater challenges in biological macromolecular crystals than in conventional small-molecule crystals. The lack of sufficient contrast of defects is often a limiting factor in x-ray diffraction topography of protein crystals. This has seriously hampered efforts to understand the mechanisms and origins associated with the formation of imperfections and the role of defects as essential entities in the bulk of macromolecular crystals. In this report, we employ a phase-sensitive x-ray diffraction imaging approach [1] for augmenting the contrast of defects in protein crystals.

## Methods and Materials

Experiments were carried out at beamline 2-BM of the Synchrotron Radiation Instrumentation Collaborative Access Team (SRI-CAT) at the APS. A Si(111) double-bounce monochromator was used to deliver an approximately monochromatic beam with an angular divergence of  $2 \times 10^{-5}$  rad and a beam pass,  $\Delta\lambda/\lambda$ , of  $\sim 1.48 \times 10^{-4}$  at a wavelength of 0.96 Å. A six-circle Huber diffractometer was employed with a scintillation detector and a charge-coupled device (CCD) camera to perform rocking-curve and imaging measurements. Well-faceted and optically defect-free tetragonal hen egg white lysozyme (HEWL) crystals grown by a batch method [2] were loaded into quartz capillaries for measurements.

## Results

Sets of the high-angular-sensitivity x-ray diffraction images of a HEWL crystal are shown in Figs. 1(a), 1(b), 1(d), and 1(e), taken with 4 4 0 [Fig. 1(c)]. The images are negatives (i.e., white regions diffract strongly, and vice versa). Figures 1(a) and 1(d) were taken at the same angular position on peak M with the camera placed  $\sim 7$  cm and 25 cm away from the sample, respectively. A number of defects, such as the dislocations D and L, are discernable in Fig. 1(a). Note the intensity variation in the strongly diffracted regions with increasing sample-to-camera distance  $R_d$ . The dislocations D, the dislocation loops (or half loops) L, and additional structural features in great detail are more clearly visible in Fig. 1(d) than in Fig. 1(a). The substantial defect contrast obtained by properly increasing  $R_d$  or defocus (in a way, by a process

similar to that used for performing the “in-line” phase contrast radiographic imaging [3, 4]) is primarily of phase contrast. Of course, in some cases, the resulting imaging patterns of defects are complex, partly as a result of the orientation and dynamical contrast effects. A number of linear features originate from the growth sector boundary GB at the top right corner, as observed in solution-grown conventional crystals. The middle crystal part, marked M in Fig. 1(d), appears to be less ordered than the near regions. The white regions [Figs. 1(a) and 1(d)] are out of diffraction when the crystal is rocked to the subpeak, which is separated from the main peak by  $0.005^\circ$ . A small crystal part (Fig. 1e) diffracts strongly instead. A number of defects, marked D in Fig. 1(e), emerge from the center of the crystal and originate from the initial nucleus. The segments of the dislocations in Fig. 1(d) are largely along the  $\langle 001 \rangle$  and  $\langle 110 \rangle$  directions, yet the subtle osmotic pressure might play a role in the dislocation configuration, given the intrinsic nature of weak macromolecular bonding. The looplike dislocations are attributed to stress/strain relief around stress centers (e.g., caused by the nonuniform trapping of impurities [5]). Such a center appears discernable in Fig. 1(b).

## Discussion

In the present cases, a defect (object) can be considered as a perturbation source that modifies the wavefront of a part of the outgoing beam diffracted at the defective region. When this modified part (the object wave) interacts with an unperturbed part (the reference wave that provides a basis from which the phase changes can be measured) diffracted from the surrounding “near-perfect” region, interference is yielded, provided the parts coherently or partially coherently correlate in space. This is the primary cause of the enhanced contrast effects. The work demonstrates that lattice defects in weakly scattering protein crystals can be effectively mapped by simply incorporating phase information of exit x-ray waves into diffraction imaging. The intensity distribution of defect images and the strength of interference effects obtained by this method correlate directly with the nature and types of defects and how well the lattices are defined, as well as the degree of coherence of the incident x-ray beam. Therefore, this imaging approach potentially allows both detailed physical defects and the correlation of

molecules in position in crystals to be evaluated in terms of varying contrast.

### Acknowledgments

Z. W. Hu wishes to thank F. De Carlo for his help with the initial setup of the CCD camera and L. Q. Chen for his help with the examination of structure factors. This research was supported by NASA. Use of the APS was supported by the U.S. Department of Energy, Office of Science, Office of Basic Energy Sciences, under Contract No. W-31-109-ENG-38.

### References

See Z. W. Hu, B. Lai, Y. S. Chu, Z. Cai, D. C. Mancini, B. R. Thomas, and A. A. Chernov, *Phys. Rev. Lett.* **87**,

148101-1 through 148101-4 (2001) for more detailed information.

[1] Z. W. Hu, P. A. Thomas, A. Snigirev, I. Snigireva, A. Souvorov, P. G. R. Smith, G. W. Ross, and S. Teat, *Nature* **392**, 690-693 (1998).

[2] B. R. Thomas, D. Carter, and F. Rosenberger, *J. Crystallogr. Growth* **187**, 499(1998).

[3] A. Snigirev, I. Snigireva, V. Kohn, S. Kuznetsov, and I. Schelokov, *Rev. Sci. Instrum.* **66**, 5486 (1995).

[4] S. W. Wilkins, T. E. Gureyev, D. Dao, A. Pogany, and A. W. Stevenson, *Nature* **384**, 335 (1996).

[5] A. A. Chernov, *Modern Crystallography III: Growth of Crystals* (Springer, Berlin, 1984).

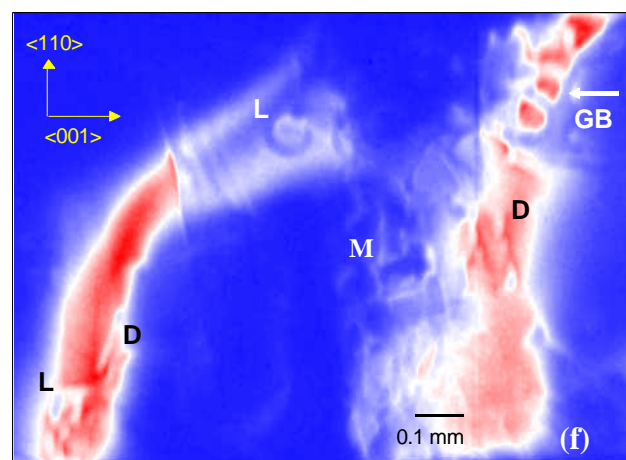
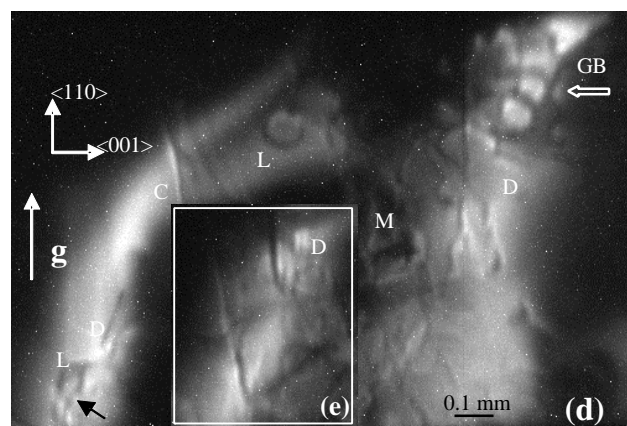
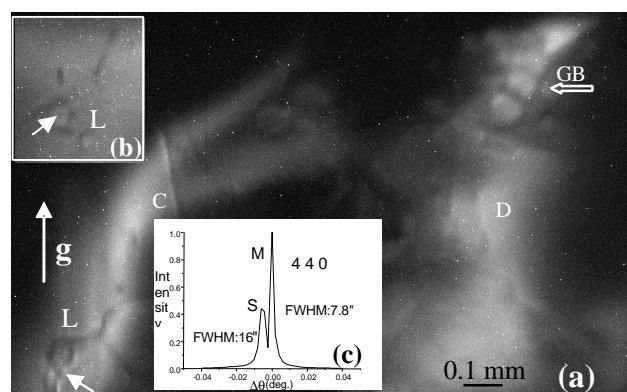


FIG. 1. Phase-sensitive diffraction images of a lysozyme crystal taken at sample-to-camera distances  $R_d$  of 7 cm (a and b) and 25 cm (d and e). A black spot marked by an arrow in (b) appears in the center of the dislocation loop L.  $g$  = the diffraction vector, GB = the growth sector boundary, and D and L = dislocations. (c) = 440 rocking curve. (f) = colored (d).